ChemPubSoc Europe

DOI: 10.1002/batt.201700004

BATTERIES & SUPERCAPS
Articles

Artificial Composite Anode Comprising High-Capacity Silicon and Carbonaceous Nanostructures for Long Cycle Life Lithium-Ion Batteries

Ben Breitung,*[a, b] Artur Schneider,[a] Venkata Sai Kiran Chakravadhanula,[b, c, d] Christian Suchomski,[e] Jürgen Janek,[a, e] Heino Sommer,[f] and Torsten Brezesinski*[a]

The use of functional nanomaterials is a common strategy to improve the mechanical and electrochemical properties of silicon anodes for secondary lithium-ion cells. Here, we report the preparation of a structurally stable composite material with a unique morphology comprising small-size silicon particles and especially branched carbonaceous nanofibers and the analysis of its cycling performance by galvanostatic measurements. This two-phase composite was obtained from pyrolysis of blended silicon/cyanamide powders. The conversion of cyanamide to turbostratic carbon, rather than graphitic carbon nitride, was unexpected and appears to be catalyzed by accidental iron nanoparticles. Although the carbon content after pyrolysis was only about 7%, half-cells using electrodes containing the silicon/carbon composite outperformed other silicon-based anode materials tested herein in terms of cyclability. After 300 cycles, they delivered two times higher capacity ($>$ 1.7 A h $g_{silicon}^{-1}$ at C/10 and $>$ 0.5 A h $g_{silicon}^{-1}$ at 1C in the 600–30 mV range when operated in constant current mode) than cells of similar loading with pristine silicon particles. The average fade rate per cycle was around 0.1% between the 10th and 300th cycles, which is notable considering that the electrode structure and composition have not yet been optimized for battery applications.

1. Introduction

In recent years, a significant increase in demand for energy storage in portable devices and electric vehicles has arisen and lithium-ion battery (LIB) technologies are widely used today to address such demand.[1] Besides the development and design of functional electrolytes and electrolyte additives, either new intercalation materials or different storage mechanisms are required to improve the energy density of state-of-the-art LIBs (e.g., to further increase their prospect for application in the automotive industry). The basic working principle of LIBs, the cell components used, including active and inactive materials, and the challenges that remain to be addressed have been described in many reviews and papers elsewhere, and thus will not be discussed here.[2]

A promising negative electrode material is silicon (Si). It has been shown to undergo electrochemical alloying with lithium (Li), leading to exceptionally high theoretical capacities (up to 4008 mA h g_{Si}^{-1} for $Li_{21}Si_5$).[3] Although there are several Li-rich silicides in the Li–Si phase diagram, $Li_{15}Si_4$, whose presence can be unambiguously inferred from the voltage (delithiation) profile, is usually observed during cycling operation.[4] Since Si also has a low average lithiation potential, it is a desirable anode material and has been widely discussed as a full or partial replacement for graphite in next generation LIBs.[5] Nevertheless, there are some showstoppers preventing the commercialization of LIBs with high-content Si anodes. The disadvantages include: low Coulombic efficiency in the first couple of cycles; kinetic limitations; and mechanical failure to name a few. In particular, the large volume changes during alloying and dealloying with Li adversely affect the stability of both the Si material itself (the shrinking and swelling creates large compressive and tensile stresses) and the solid electrolyte interphase (SEI), which ultimately leads to continuous lithium loss at the anode side and causes increases in contact and

[a] Dr. B. Breitung, Dr. A. Schneider, Prof. J. Janek, Dr. T. Brezesinski
Battery and Electrochemistry Laboratory
Institute of Nanotechnology
Karlsruhe Institute of Technology
Hermann-von-Helmholtz-Platz 1,
76344 Eggenstein-Leopoldshafen (Germany)
E-mail: ben.breitung@kit.edu
torsten.brezesinski@kit.edu
[b] Dr. B. Breitung, Dr. V. S. K. Chakravadhanula
Institute of Nanotechnology
Karlsruhe Institute of Technology
Hermann-von-Helmholtz-Platz 1,
76344 Eggenstein-Leopoldshafen (Germany)
[c] Dr. V. S. K. Chakravadhanula
Karlsruhe Nano Micro Facility
Karlsruhe Institute of Technology
Hermann-von-Helmholtz-Platz 1,
76344 Eggenstein-Leopoldshafen (Germany)
[d] Dr. V. S. K. Chakravadhanula
Helmholtz Institute Ulm for Electrochemical Energy Storage
Helmholtzstraße 11,
89081 Ulm (Germany)
[e] Dr. C. Suchomski, Prof. J. Janek
Institute of Physical Chemistry
Justus-Liebig-University Giessen
Heinrich-Buff-Ring 17,
35392 Gießen (Germany)
[f] Dr. H. Sommer
BASF SE
67056 Ludwigshafen (Germany)
Supporting Information and the ORCID identification number(s) for the author(s) of this article can be found under:
https://doi.org/10.1002/batt.201700004

charge transfer resistances.[3a,4b,5b,6] Such processes strongly afflict Si-based LIBs, making their prevention crucial for the advancement of the technology. However, the problem of particle fracture apparently can be mitigated to some degree by use of small-size Si particles, and with that also the capacity fade behavior.[7] Besides, electron microscopy analysis has shown that the critical fracture diameter is different for amorphous and crystalline Si materials, and this is valid as well for the kinetics.[8]

From a materials perspective (not considering the binder and conductive additives), predominantly coated Si particles and composites comprising electrically conductive and somewhat flexible support materials have been tested over the course of the past decade in an attempt to accommodate the volume expansion and to improve kinetics.[9] Those that stand out in this regard are carbon and carbonaceous polymeric materials.[9,10] Apart from carbon nanotubes and graphene, pyrolyzed carbons derived from organic precursors show promise as coating or matrix materials, for example, to achieve three-dimensional composite structures with intimate contact between the two (or more) phases. Such materials/architectures often exhibit superior mechanical properties to traditional physical mixtures while also ensuring efficient electron transfer and transport through the electrode.

In this work, we compare the cyclability of medium loading half-cells using different Si anode materials and show that even small amounts of carbonaceous nanostructures can help to considerably improve the overall performance. Specifically, a newly synthesized precursor-derived Si/C composite was found to have good Li-storage properties; it outperformed all of the other materials tested. This seems to be due in part to its unique structure and morphology, which interestingly cannot be mimicked or replicated by using blends of Si particles and similarly structured carbon.

2. Results and Discussion

The morphology, microstructure, and composition of the resulting material from the pyrolysis of a 1:1 mixture of nanoscale Si and cyanamide (CH_2N_2) in a stainless steel reactor were investigated by a combination of electron microscopy, Raman and FTIR spectroscopy, TGA, and PXRD. Bright-field TEM images at different magnifications (Figures 1a–d) reveal a heterogeneous distribution of partially agglomerated polydisperse Si particles in carbonaceous (C) nanostructures. Nanofibers in particular are clearly visible, while some of the Si particles are also coated by a thin carbon shell. In recent years, it has been shown that graphitic carbon nitride (C_3N_4) can be prepared from pyrolysis of cyanamide under inert atmosphere.[11] The formation of carbonaceous material is thus somewhat surprising and suggests that the process is catalyzed either by the Si particles themselves or by impurities in the reactants and/or reactor vessel. Apart from the Si/C composite, sub-10 nm carbon-encapsulated particles were also found and identified by energy-dispersive X-ray spectroscopy as iron (Fe). Note that Fe is a common catalyst in the chemical vapor

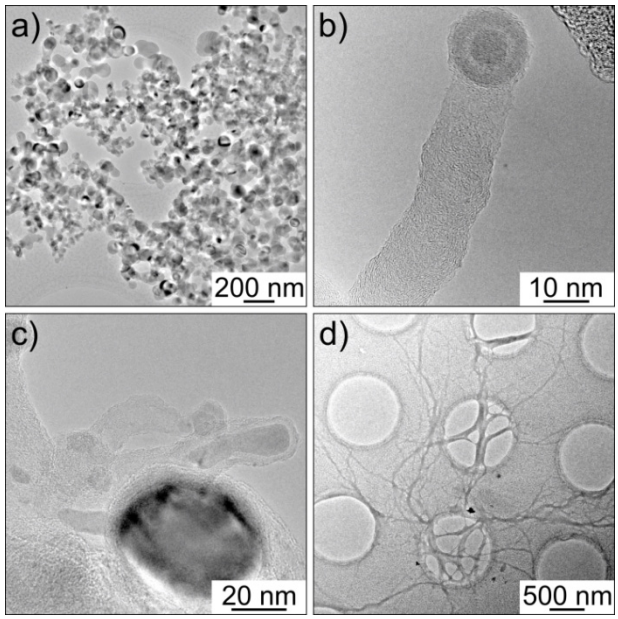

Figure 1. Electron microscopy of cyanamide-derived Si/C composite. (a, d) Low-magnification TEM images showing polydisperse Si particles of spherical geometry and carbonaceous nanofibers. (b, c) High-resolution TEM images showing Fe nanoparticles as active catalyst centers and carbon-coated Si.

deposition growth of carbon nanostructures.[12] Since Fe nanoparticles were not intentionally added to the reaction mixture, they must have formed during pyrolysis, presumably through chemical reaction with the stainless steel reactor. Interestingly, Fe nanoparticle formation did not occur in the absence of Si (within the limits of detection), thereby indicating that their origin is clearly linked to processes involving Si. Previous XPS studies by Erk et al. have shown that commercial Si materials typically exhibit different surface functional groups (mainly OH and Cl groups), which might be involved in the formation of Fe nanoparticles.[13] Although more efforts are needed to unravel the underlying mechanism(s), the presence of randomly dispersed catalyst particles appears to play a key role in the conversion reaction of cyanamide to carbon. Notably, some of the loose carbonaceous material could be separated from the final composite by ultrasonication in toluene. As observed through TEM, the nanofibers are highly branched and have diameters <200 nm and a length of several micrometers, leading to relatively high aspect ratios.

Raman spectra obtained on pristine Si particles and cyanamide-derived Si/C composite are depicted in Figure 2a. The major band centered at 515 cm^{-1} and the multiphonon peaks in the range between 200 cm^{-1} and 1000 cm^{-1} are characteristic of bulk crystalline Si. Additional bands at 1365 cm^{-1} and 1585 cm^{-1} are seen for the Si/C composite that correspond to the D and G modes of turbostratic carbon, respectively. Using the intensity ratio of the latter bands, the lateral extent of the graphene layers was estimated to 4–5 nm.[14]

FTIR spectra of C_3N_4, Si, and Si/C are presented in Figure 2b. The absorption around 1640 cm^{-1} and those at 1350–1000 cm^{-1} can be assigned to C=N and C–N stretching

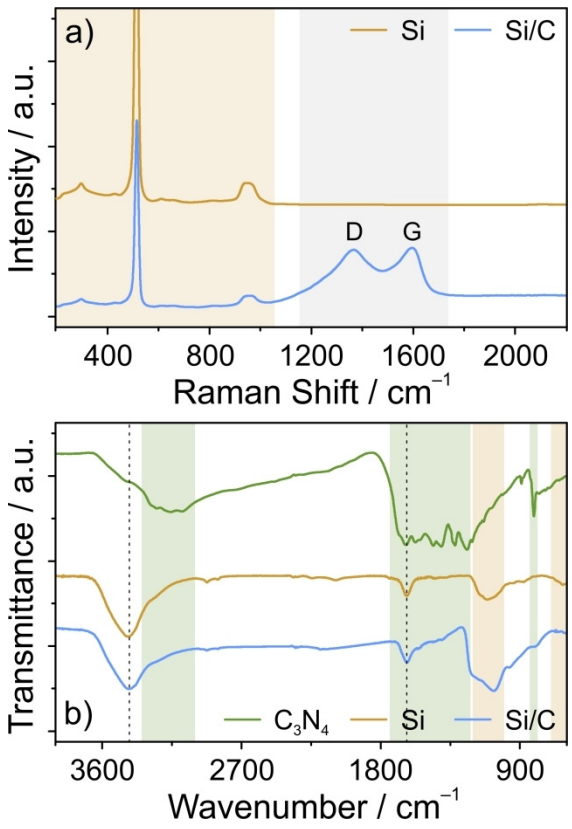

Figure 2. (a) Raman spectra obtained on pristine Si particles and cyanamide-derived Si/C composite. (b) KBr-pellet FTIR spectra of C_3N_4, Si, and Si/C showing that the material after pyrolysis contains only trace levels of C_3N_4, if at all. The gray shaded area represents the C Raman region, while Si Raman/IR and C_3N_4 IR regions are highlighted in orange and green, respectively. The dashed black lines in (b) indicate OH bending and stretching vibrations from adsorbed H_2O.

vibrations, respectively. The bands at 810 cm^{-1}, 1410 cm^{-1}, 1465 cm^{-1}, and 1575 cm^{-1} are due to s-triazine ring vibrations. Moreover, the C_3N_4 data show stretching and deformation vibrations of NH and NH_2 groups at 3300–3100 cm^{-1} and 1680 cm^{-1}.[15] For both Si and Si/C, the strong bands at 1200–1000 cm^{-1} and those below 1000 cm^{-1} (especially at 875 cm^{-1} and 620 cm^{-1}) can be attributed to Si–O stretching vibrations and Si two-phonon modes, respectively.[16] In addition, there are intense bands centered at 3420 cm^{-1} (OH stretching vibration) and 1630 cm^{-1} (OH bending vibration) due to adsorbed H_2O. Overall, we conclude from the Raman and FTIR results that either no or only traces of C_3N_4 are present in the Si/C composite. Nevertheless, even if it contains some, the total amount is much smaller compared to that of carbon, and thus can be considered insignificant, at least with respect to electrochemical cycling (the same applies to the Fe nanoparticles). The carbon content was determined by TGA to be 6–7 wt.–% using pristine Si particles as reference material.

Representative PXRD patterns of the different Si-based materials are depicted in Figure S1 (Supporting Information). As expected, they only show distinct reflections of cubic Si with space group $Fd\bar{3}m$ (ICSD reference code 51688) and further indicate that the average crystallite size (approx. 23 nm) remains unaffected by the pyrolysis reaction.

The Li-storage properties of the Si particles with and without cyanamide-derived carbonaceous nanostructures were examined by galvanostatic cycling in coin-type cells. The areal Si loading was kept similar for all of the electrodes tested at around 1 mg cm^{-2}. Instead of ethylene carbonate, fluoroethylene carbonate (FEC) was used as co-solvent in the electrolyte. The reason is that FEC has been shown to not only promote the SEI formation on Si and other LIB materials, but also to favorably affect the gassing behavior of such cells.[6c,d,f,17] Ultimately, this leads to less side reactions and improved stability during cycling operation. The cells were first subjected to a formation (or activation) process at low C-rate to address the bulk of the electrodes as effectively as possible and, more importantly, to allow formation of a robust SEI. Then, they were cycled either in CC/CV or CC mode in the voltage range between 600 mV and 30 mV. The details of the cycling protocol used are given in the Experimental Section and Table S1 (Supporting Information). Specific lithiation capacities and Coulombic efficiencies during 200 cycles are shown in Figures 3a and b. The capacity for both the cells with pristine Si particles and Si/C composite drops from initially about 4.3 A h g_{Si}^{-1} to 2.2 and 2.5 A h g_{Si}^{-1}, respectively, within 10 cycles and stabilizes thereafter (note that the specific capacity values can be directly translated into areal capacities of unit mA h cm^{-2}). This is due to different reasons, including prolonged SEI formation and SEI resistance buildup over multiple cycles, irreversible electrochemical reactions of Li with the native Si oxide layer, but also because the voltage window was narrowed for stability reasons and the C-rate was increased after the initial cycles.[18] However, as is evident from Figure 3a, the capacity reaches fairly stable values during the following cycles in the case of the Si/C composite. Cells using this material exhibit significantly improved capacity retention and, after 200 cycles, they have nearly two times higher capacity than cells with pristine Si particles. The same is also valid for higher cycle numbers (see Figure S2 of the Supporting Information). The specific capacity decreases by 24% from the 10th to 200th cycle, corresponding to a relatively low average fade rate per cycle of 0.13% or 3.2 mA h g_{Si}^{-1} (compare to 0.26% or 5.8 mA h g_{Si}^{-1} for pristine Si particles). In addition, the data indicate that a reasonable cycling performance can be achieved already for noncomplex electrode structures through careful choice of electrolyte and binder system.[13] They also demonstrate that electrodes containing the Si/C composite exhibit better kinetics; they are capable of delivering capacities >0.5 A h g_{Si}^{-1} at 1C, yet the 3C performance is poor. The result that the capacity degradation at 1C is much faster in earlier cycles (see also Figure S2 of the Supporting Information) is probably related to the fact that side reactions as well as structural and/or morphological changes are most pronounced during the first couple of dozen cycles.

Voltage profiles for the initial and later cycles at different C-rates are depicted in Figure S3 (Supporting Information). These curves show the characteristics that are expected for Si anodes but, more importantly, they confirm the lower overvoltage for

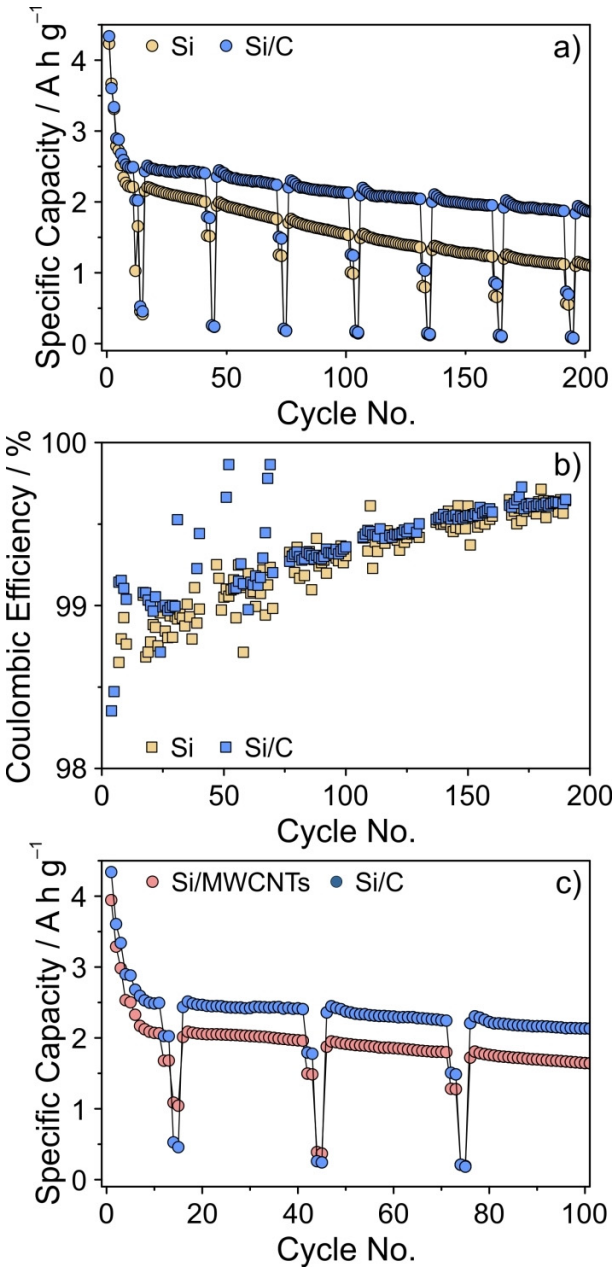

Figure 3. Galvanostatic cycling performance of Li cells using electrodes containing pristine Si particles, cyanamide-derived Si/C composite, and blended Si/MWCNTs. (a, c) Specific lithiation capacity and (b) Coulombic efficiency as a function of cycle number. After low C-rate formation, the cells were cycled between 600 mV and 30 mV. Except during rate capability testing, the charge and discharge C-rate was C/2.

the electrochemical alloying and dealloying with Li and improved kinetics in the case of the Si/C composite. Overall, this provides an explanation for the better Li-storage properties.

Inspection of the evolution of the Coulombic efficiency with cycle number also corroborates the enhanced cyclability (reversibility, stability etc.). The initial Coulombic efficiency is 81% and 85% for Si/C and Si, respectively. The slightly greater capacity loss seen for cells containing the composite material is indicative of more irreversible side reactions such as SEI formation during the first charge (lithiation). However, this was somewhat expected given the nature of the cyanamide-derived carbon. Still, on average, the Coulombic efficiency, which is >99% after 10 cycles and increases to over 99.6% with prolonged cycling, is higher when the Si/C composite is used (Figure 3b). Besides, it is more stable or, in other words, shows less scatter roughly from the 75th cycle on, which is another clear indication of the improvement in stability.

Since the nanostructures observed by electron microscopy (Figure 1) are partly reminiscent of carbon nanotube networks, we tested whether a similar cycling performance can be achieved for physical mixtures (blends) of Si particles and MWCNTs. The carbon content was chosen to be identical to that of the Si/C composite. A direct comparison of the capacity retention over the first 100 cycles is depicted in Figure 3c. Most notably, the Si/MWCNTs blended electrodes deliver considerably lower specific capacities (by 0.4–0.5 A h g_{Si}^{-1}), the reason of which is unclear. In addition, the capacity fade rate between the 10th and 100th cycles is higher (4.7 vs 3.9 mA h g_{Si}^{-1} per cycle). However, the overall performance is greatly improved compared to cells using pristine Si particles, showing a loss in capacity >0.6 A h g_{Si}^{-1} (7.4 mA h g_{Si}^{-1} per cycle) over the same number of cycles. The observed trends in Coulombic efficiency are similar, although the Si/MWCNTs data scatter more, particularly in later cycles (see Figure S4 of the Supporting Information). Also worth mentioning is that the first cycle efficiency is around 81%, thus confirming the above conclusions. Collectively, our research data establish that the electrochemical behavior of the Si/C composite in Li cells cannot be mimicked or replicated by simply using Si/MWCNTs blends, which further emphasizes the unique structure and/or composition of the cyanamide-derived material employed in this work.

As discussed above, both the capacity and longevity of cells can be significantly increased when using the Si/C composite. However, it should be noted that the performance is not yet satisfactory for practical LIB applications. While electrochemical testing revealed a lower overvoltage during prolonged cycling and better kinetics, this does not necessarily explain the improved capacity retention. For high-capacity Si anodes, the fading is often directly related to the morphological and mechanical instability of the electrode itself. In order to gain more insight into the structural evolution of electrodes containing the Si/C composite, we decided to look at them before and after cycling using SEM. Unfortunately, surface imaging was not possible after a larger number of cycles because of their high reactivity, even when discharged (delithiated) to ≥1 V (probably due to remaining lithium silicides in the electrode). Nevertheless, SEM data could be acquired before and after the low C-rate formation cycles, and they already provide some idea of what makes the cyanamide-derived material superior in terms of cyclability. From the top-view images in Figures 4a and b, it can be clearly seen that the particles largely remain their original size and shape and the overall electrode morphology is well preserved (see also Figure S5 of the Supporting Information for SEM images at different magnifications). As expected, some microcracking occurs due to continuous shrinking and swelling of the Si

particles. However, interestingly, these cracks are bridged to some extent by nanofibers, some of which are highlighted in Figure 4c. This in turn suggests that the different electrode regions remain electrochemically active (electronically connected), even during material displacement, which is in agreement with the finding that cells using the Si/MWCNTs blended electrodes exhibit improved performance than those with pristine Si particles. But regardless, the effect of nanofiber branching on the cycling stability and the fact that some fraction of the Si particles are coated by a thin turbostratic carbon shell should not be underestimated and deserves more attention and study.

3. Conclusions

In this work, the lithium-storage properties of a new silicon-based anode material were evaluated using galvanostatic measurements at various current rates. For reasons that are not yet fully understood, the pyrolysis of cyanamide in the presence of silicon particles in a stainless steel reactor did not yield the anticipated graphitic carbon nitride, but rather resulted in formation of high-aspect-ratio carbonaceous nanostructures. Structural analysis confirmed the turbostratic nature of the carbon; the morphology and crystallinity of the silicon particles remained virtually unaffected by the pyrolysis reaction. Half-cells using electrodes containing the cyanamide-derived silicon/carbon composite outperformed similarly loaded cells with either pristine silicon particles or blends with multiwalled carbon nanotubes in terms of cyclability. Overall, the results of the current study indicate that interpenetrating network structures of silicon particles and branched carbonaceous nanostructures show promise for electrochemical energy storage applications and deserve further investigation. In the future, such electrode materials might become alternatives to conventional graphite or silicon/graphite blended anodes if their properties can be improved and ideally tailored to specific requirements. However, because low Coulombic efficiency, particularly in the initial cycle, is one of the showstoppers of high-content silicon anodes, the successful implementation of nanoscale materials, the use of which appears to be necessary (at least in part), is challenging.

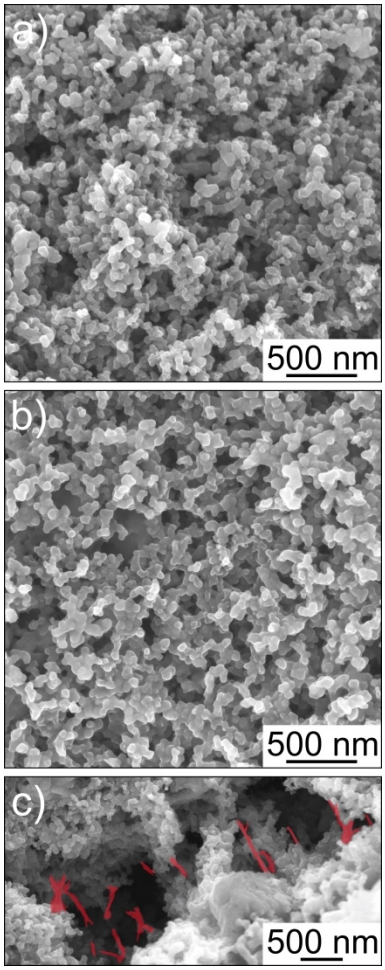

Figure 4. Top-view SEM images of cyanamide-derived Si/C composite electrodes (a) before and (b, c) after the low C-rate formation cycles. (c) Microcracks in the electrode are bridged by nanofibers, some of which are highlighted in red.

Experimental Section

Materials Synthesis and Electrode Preparation

Si/C composite material was prepared via facile one-pot pyrolysis reaction. In a typical synthesis, Si particles of average size $\leq$50 nm (250 mg, 98%, Alfa Aesar) and cyanamide (CH_2N_2, 250 mg, 99%, Sigma Aldrich) were placed in a stainless steel reactor (Swagelok) inside an Ar-filled glove box (MBraun). Then, the reactor was heated in a muffle furnace at 575 °C for 5 h (3 °C min^{-1} heating rate). After cooling to room temperature, the pressure that developed due to formation of gaseous side products was carefully released and the reactor was opened. The resulting fine dark-brown powder was collected and used without further post-treatment.

Electrodes were prepared by slurry casting onto 18 μm Cu foil (Gould Electronics), followed by drying at 80 °C in vacuum for 12 h. A homogenous dispersion was achieved by thoroughly mixing either pristine Si particles, cyanamide derived Si/C composite, or blended Si/multiwalled carbon nanotubes (MWCNTs, 6–9 nm × 5 μm, >95%, Sigma-Aldrich) (63 wt.–%), Super C65 carbon black additive (22 wt.–%, Timcal), and poly(vinyl alcohol) Selvol 425 binder (15 wt.–%, Sekisui) in H_2O using a planetary centrifugal mixer (Thinky Corporation). For comparison reasons, the areal loading was always set to around 1 mg_{Si} cm^{-2}.

Cell Testing and Characterization Methods

Coin-type cells consisting of Si-based working electrode, GF/D type glass microfiber separator (Whatman) soaked with electrolyte solution, and 600 μm Li foil counter electrode (Albemarle Germany GmbH) were assembled inside an Ar-filled glove box (MBraun). The electrodes and the separator had diameters of 13 mm and 17 mm, respectively, and the electrolyte solution used was 1 M $LiPF_6$ in 1:1 by weight fluoroethylene carbonate (Solvay) and ethyl methyl carbonate (BASF SE). The H_2O content was determined to be equal to or less than 10 ppm. Galvanostatic testing was performed at different C-rates, with 1C = 4008 mA g_{Si}^{-1}, and at a stable temperature of 25 °C using a BINDER cooled incubator and a MACCOR

Series 4000 cycler (Tulsa). After the initial low C-rate cycles between 1000 mV and 10 mV and 600 mV and 30 mV were completed, the cells were cycled at C/2 charge (lithiation) and discharge (delithiation) with cutoff voltages of 30 mV and 600 mV, respectively. A constant voltage step at the cutoff voltages was applied until the current dropped below C/20 (constant current/constant voltage [CC/CV] mode), except for rate performance testing, where the discharge C-rate was varied from C/10 to 3C (CC mode). More details are given in Tab. S1 (Supporting Information).

Scanning electron microscopy (SEM) was performed on a MERLIN microscope (Carl Zeiss) operated at 5–10 keV. Transmission electron microscopy (TEM) was performed on an aberration corrected FEI Titan 80–300 microscope operated at 300 keV. The samples were dispersed on amorphous carbon-coated Cu grids (Quantifoil). Powder X-ray diffraction (PXRD) was performed in reflection mode on a Bruker AXS D8 Advance (Cu–Kα radiation source) equipped with a LynxEye Si strip detector. Raman spectroscopy was performed on a SENTERRA dispersive Raman microscope equipped with a YAG:Nd laser and an MPlan N 50× Olympus objective. Thermogravimetric analysis (TGA) was performed on a NETZSCH TG 209 F1 Libra. Fourier transform infrared (FTIR) spectroscopy was performed on a Bruker IFS-48 spectrometer.

Acknowledgements

This study is part of the projects being funded within the BASF International Network for Batteries and Electrochemistry.

Conflict of Interest

The authors declare no conflict of interest.

Keywords: Silicon · carbon · nanostructures · lithium-ion battery · anode

[1] a) G. E. Blomgren, *J. Electrochem. Soc.* **2017**, *164*, A5019–A5025; b) S.-T. Myung, F. Maglia, K.-J. Park, C. S. Yoon, P. Lamp, S.-J. Kim, Y.-K. Sun, *ACS Energy Lett.* **2017**, *2*, 196–223.

[2] a) P. G. Bruce, B. Scrosati, J.-M. Tarascon, *Angew. Chem. Int. Ed.* **2008**, *47*, 2930–2946; *Angew. Chem.* **2008**, *120*, 2972–2989; b) M. Armand, J.-M. Tarascon, *Nature* **2008**, *451*, 652–657; c) B. Scrosati, J. Garche, *J. Power Sources* **2010**, *195*, 2419–2430; d) J. B. Goodenough, Y. Kim, *Chem. Mater.* **2010**, *22*, 587–603; e) B. Dunn, H. Kamath, J.-M. Tarascon, *Science* **2011**, *334*, 928–935; f) W. Liu, P. Oh, X. Liu, M.-J. Lee, W. Cho, S. Chae, Y. Kim, J. Cho, *Angew. Chem. Int. Ed.* **2015**, *54*, 4440–4457; *Angew. Chem.* **2015**, *127*, 4518–4536; g) A. Manthiram, J. C. Knight, S.-T. Myung, S.-M. Oh, Y.-K. Sun, *Adv. Energy Mater.* **2016**, *6*, 1501010; h) J. Xu, F. Lin, M. M. Doeff, W. Tong, *J. Mater. Chem. A* **2017**, *5*, 874–901; i) M. D. Radin, S. Hy, M. Sina, C. Fang, H. Liu, J. Vinckeviciute, M. Zhang, M. S. Whittingham, Y. S. Meng, A. Van der Ven , *Adv. Energy Mater.* **2017**, *7*, 1602888; j) L. de Biasi, A. O. Kondrakov, H. Geßwein, T. Brezesinski, P. Hartmann, J. Janek, *J. Phys. Chem. C* **2017**, *121*, 26163–26171.

[3] a) U. Kasavajjula, C. Wang, A. J. Appleby, *J. Power Sources* **2007**, *163*, 1003–1039; b) C.-M. Park, J.-H. Kim, H. Kim, H.-J. Sohn, *Chem. Soc. Rev.* **2010**, *39*, 3115–3141; c) N. Nitta, F. Wu, J. T. Lee, G. Yushin, *Mater. Today* **2015**, 18, 252–264.

[4] a) H. Wu, Y. Cui, *Nano Today* **2012**, *7*, 414–429; b) M. N. Obrovac, V. L. Chevrier, *Chem. Rev.* **2014**, *114*, 11444–11502; M. Zeilinger, I. M. Kuryliyshyn, U. Häussermann, T. F. Fässler, *Chem. Mater.* **2013**, *25*, 4623–4632.

[5] a) R. Dash, S. Pannala, *Sci. Rep.* **2016**, *6*, 27449; b) S. Chae, M. Ko, K. Kim, K. Ahn, J. Cho, *Joule* **2017**, *1*, 47–60.

[6] a) L. Y. Beaulieu, K. W. Eberman, R. L. Turner, L. J. Krause, J. R. Dahn, *Electrochem. Solid-State Lett.* **2001**, *4*, A137-A140; b) W.-J. Zhang, *J. Power Sources* **2011**, *196*, 13–24; c) C. Xu, F. Lindgren, B. Philippe, M. Gorgoi, F. Björefors, K. Edström, T. Gustafsson, *Chem. Mater.* **2015**, *27*, 2591–2599; d) R. Jung, M. Metzger, D. Haering, S. Solchenbach, C. Marino, N. Tsiouvaras, C. Stinner, H. A. Gasteiger, *J. Electrochem. Soc.* **2016**, *163*, A1705-A1716; e) B. Breitung, P. Baumann, H. Sommer, J. Janek, T. Brezesinski, *Nanoscale* **2016**, *8*, 14048–14056; f) A. Schiele, B. Breitung, T. Hatsukade, B. B. Berkes, P. Hartmann, J. Janek, T. Brezesinski, T. *ACS Energy Lett.* **2017**, *2*, 2228–2233.

[7] a) J. Graetz, C. C. Ahn, R. Yazami, B. Fultz, *Electrochem. Solid-State Lett.* **2003**, *6*, A194–A197; b) X. H. Liu, L. Zhong, S. Huang, S. X. Mao, T. Zhu, J. Y. Huang, *ACS Nano* **2012**, *6*, 1522–1531; c) M. Gu, Y. Li, X. Li, S. Hu, X. Zhang, W. Xu, S. Thevuthasan, D. R. Baer, J.-G. Zhang, J. Liu, C. Wang, *ACS Nano* **2012**, *6*, 8439–8447; d) J. B. Cook, H.-S. Kim, T. C. Lin, S. Robbennolt, E. Detsi, B. S. Dunn, S. H. Tolbert, *ACS Appl. Mater. Interfaces* **2017**, *9*, 19063–19073.

[8] M. T. McDowell, S. W. Lee, J. T. Harris, B. A. Korgel, C. Wang, W. D. Nix, Y. Cui, *Nano Lett.* **2013**, *13*, 758–764.

[9] X. Zuo, J. Zhu, P. Müller-Buschbaum, Y.-J. Cheng, *Nano Energy* **2017**, *31*, 113–143.

[10] a) S.-H. Ng, J. Wang, D. Wexler, K. Konstantinov, Z.-P. Guo, H.-K. Liu, *Angew. Chem. Int. Ed.* **2006**, *45*, 6896–6899; *Angew. Chem.* **2006**, *118*, 7050–7053; b) N. Liu, H. Wu, M. T. McDowell, Y. Yao, C. Wang, Y. Cui, *Nano Lett.* **2012**, *12*, 3315–3321; c) Y.-S. Hu, R. Demir-Cakan, M.-M. Titirici, J.-O. Müller, R. Schlögl, M. Antonietti, J. Maier, *Angew. Chem. Int. Ed.* **2008**, *47*, 1645–1649; *Angew. Chem.* **2008**, *120*, 1669–1673; d) X. Su, W. Wu, J. Li, X. Xiao, A. Lott, W. Lu, B. W. Sheldon, J. Wu, *Adv. Energy Mater.* **2014**, *4*, 1300882.

[11] a) E. Kroke, M. Schwarz, M. *Coord. Chem. Rev.* **2004**, *248*, 493–532; b) M. Groenewolt, M. Antonietti, *Adv. Mater.* **2005**, *17*, 1789–1792; c) A. Thomas, A. Fischer, F. Goettmann, M. Antonietti, J.-O. Müller, R. Schlögl, J. M. Carlsson, *J. Mater. Chem.* **2008**, *18*, 4893–4908.

[12] a) M. Jose-Yacaman, M. Miki-Yoshida, L. Rendon, J. G. Santiesteban, *Appl. Phys. Lett.* **1993**, *62*, 657–659; b) W. Z. Li, S. S. Xie, L. X. Qian, B. H. Chang, B. S. Zou, W. Y. Zhou, R. A. Zhao, G. Wang, *Science* **1996**, *274*, 1701–1703.

[13] C. Erk, T. Brezesinski, H. Sommer, R. Schneider, J. Janek, *ACS Appl. Mater. Interfaces* **2013**, *5*, 7299–7307.

[14] F. Tuinstra, J. L. Koenig, *J. Chem. Phys.* **1970**, *53*, 1126–1130.

[15] V. N. Khabashesku, J. L. Zimmerman, J. L. Margrave, *Chem. Mater.* **2000**, *12*, 3264–3270.

[16] a) I. W. Boyd, *Appl. Phys. Lett.* **1987**, *51*, 418–420; b) O. Pluchery, J.-M. Costantini *J. Phys. D: Appl. Phys.* **2012**, *45*, 495101.

[17] a) S. Dalavi, P. Guduru, B. L. Lucht, *J. Electrochem. Soc.* **2012**, *159*, A642-A646; b) E. Markevich, G. Salitra, D. Aurbach, *ACS Energy Lett.* **2017**, *2*, 1337–1345.

[18] a) S. Xun, X. Song, L. Wang, M. E. Grass, Z. Liu, V. S. Battaglia, G. Liu, *J. Electrochem. Soc.* **2011**, *158*, A1260-A1266; b) A. Tokranov, R. Kumar, C. Li, S. Minne, X. Xiao, B. W. Sheldon, *Adv. Energy Mater.* **2016**, *6*, 1502302; c) B. Breitung, N. Aguiló-Aguayo, T. Bechtold, H. Hahn, J. Janek, T. Brezesinski, *Sci. Rep.* **2017**, *7*, 13010.

Manuscript received: December 13, 2017
Accepted article published: January 22, 2018
Version of record online: February 26, 2018